

## Aero-Structural Optimization of Sailplane Wings

Andre C. Marta\* and Bruno J. P. Cadete†

\* Instituto Superior Técnico, Lisboa, Portugal, andre.marta@ist.utl.pt

† Estado-Maior da Força Aérea, Amadora, Portugal, rantanplan.afa@gmail.com

### Abstract

This paper presents a framework for the multi-disciplinary design analysis and optimization of sailplane wings. The approach used in the multi-disciplinary optimization framework uses a multi-disciplinary feasible architecture. The geometric parametrization method employed follows a free-form deformation method. To solve the aero-structural problem, a panel method coupled with a finite-element solver is implemented. The coupled non-linear system is solved using an approximate Newton-Krylov approach. The optimization algorithm uses sequential quadratic programming, where the gradients are evaluated using the adjoint method. A real sailplane wing, based on the LET L-23 Super Blaník from the Portuguese Air Force, is used as test case. Single disciplinary analyses assess the capabilities of the disciplinary modules of the framework. Results are presented for a drag minimization problem using aerodynamic and multi-disciplinary optimizations. They reveal important trade-offs between disciplinary optimum and multi-disciplinary optimum at the preliminary design stage.

**Keywords:** Multi-disciplinary optimization, Adjoint method, Coupled analysis, Free-form deformation method, Panel method, Finite-element method.

### 1 Introduction

In aircraft design, several disciplines have to be considered, ranging from aerodynamics, structures, propulsion or controls down to aesthetics. Typically, the coupling of the disciplines is only handled in the latter stages of the design. This method has been successfully used for the last 30 years, mostly because aircraft configurations have not changed significantly and designers have built up specific know-how and expertise.

However, with the emergence of a new generation of aircrafts with revolutionary concepts, such as the blended-wing body, where the performance depends on system integration, a new design paradigm is being considered using multi-disciplinary optimization (MDO).

The use of MDO in aircraft design is relatively recent. In fact, it has only fully emerged as a technique viable for aircraft design in the last two decades, driven by the growth in computational power, the maturity of accurate flow physics analysis and the efficient optimization algorithms offered by operations research.

This paper focuses on the coupling of two of the most important disciplines in aircraft design, aerodynamics and structures, in particular in the design of wings.

The topic of aero-structural optimization of wings is specially relevant for the Portuguese Air Force. At the present time, the Air Force Academy is involved in unmanned aerial vehicle (UAV) projects like PERSEUS [1] or PITVANT [2], that may be-

nefit from using MDO early in the design stages of aircraft project.

The test case chosen was one of the instruction sailplanes used in the Air Force Academy, the LET L-23 Super Blaník. Even though it is relatively simple design aircraft, it presents an interesting subject for the research in the multi-disciplinary field since sailplanes are designed to have strong and flexible wings and great flight performance.

The paper is split in three main sections. The first section contains a concise literature review about aircraft design and MDO. Then, the aerodynamic and structural models used in the simulations are explained, and the MDO framework detailed. Finally, this framework is exercised, both in single analysis and in multi-disciplinary optimization modes.

### 2 Background

#### 2.1 Aircraft design

Since 1970's, the evolution of sailplanes has been following the exponential evolution of structural engineering, material science, computational fluid dynamics (CFD) and electronics. Many modern sailplanes are manufactured in new composite materials such as glass fiber and carbon fiber, which provide greater strength at lower weight. Also advances in CFD, allowed the development of new wing and airfoils shapes.

The principles of flight for sailplanes are the same as for all aircrafts: it is the action of forces on the entire vehicle that allows it to stay airborne. As

the wing exerts a force on the air to change its direction, the air exerts a force on the wing, equal in size but opposite in direction. The resultant force is obtained by integrating  $p$  and the wall stress  $\tau$  over the wing surface. Lift  $L$  and drag  $D$  are the force components in the normal and stream-wise flow directions, respectively. In aerodynamics, the dimensionless force coefficients, lift and drag coefficients, are defined as

$$C_L \equiv \frac{L}{q_\infty S} \quad \text{and} \quad C_D \equiv \frac{D}{q_\infty S}, \quad (1)$$

where the free-stream dynamic pressure is defined as  $q$ , being  $q_\infty$  the free-stream condition.

Drag results from three main sources: form drag, induced drag and compressibility drag. The compressibility drag effect is negligible in soaring flight, as the speeds involved are too low to cause significant compressibility of the incident airflow. Therefore, the compressibility effect is neglected in this work.

The efficiency in gliding can be measured by the maximum range or maximum endurance. Assuming that the sailplane is at equilibrium, the equations of motion are

$$\begin{aligned} D - W \sin(\gamma) &= m\dot{V} = 0, \\ L - W \cos(\gamma) &= mV_S = 0, \end{aligned} \quad (2)$$

where  $\gamma$  is the flight path angle and  $V_S = V \sin(\gamma)$  is the sinking speed. Dividing one equation by the other, the relation between the flight path angle and the  $L/D$  ratio arises,  $\tan(\gamma) = -D/L = -1/(L/D)$ . This expression gives a negative flight path angle as would be expected in gliding. Thus, defining glide angle as the negative of the flight path angle, the expression turns to  $\tan(\gamma_1) = 1/(L/D)$ , where the  $\gamma_1$  is the glide angle. Therefore, this angle is independent of the weight and its lowest value corresponds to the higher  $L/D$  ratio.

The gliding range,  $R$ , corresponds to the longest distance traveled horizontally during the glide descent. Assuming an initial altitude,  $h_1$  and a ground altitude,  $h_2$ , it can be calculated as

$$R = \frac{h_1 - h_2}{\tan \gamma_1} = \frac{L}{D}(h_1 - h_2). \quad (3)$$

Here the ratio  $L/D$  is also called gliding ratio.

Gliding endurance consists of achieving the longest duration of flight. For that to be possible, the gliding angle has to be kept at a minimum, thus, generating a minimum sinking speed. Mathematically, this speed is given as

$$V_S = V \sin(\gamma) = -V \frac{D}{W} \approx -\sqrt{\frac{W}{1/2\rho S} \frac{C_D}{C_L^3}}. \quad (4)$$

As the gliding angle is usually small, a small angle assumption ( $L = W \cos(\gamma) \approx W$ ) can be made.

To minimize the sinking rate (maximize endurance), the quantity  $C_D/C_L^3$  and the weight must be minimized.

These two measures of performance are important as they configure two possible optimization problems: one, where the objective is to maximize the range (by maximizing the  $L/D$  ratio), the other, where the endurance is maximized (by minimizing the drag and the weight).

## 2.2 Multi-disciplinary Design Optimization

An aircraft is a multi-disciplinary system as its analysis often require several fields of expertise. Performing computational analysis, together with numerical optimization, made MDO emerge as one of the fields of engineering that can provide optimal solutions to aircraft design problems.

The first surveys on MDO problems and approaches were published by the AIAA [3]. Two years later, Sobieski [4] showed that MDO could be used as an efficient way to overcome the computational challenges on a new emerging method for aircraft conceptual design. During the following years, various papers were published that examined and tested one or various MDO architectures, as for their method of defining the problem formulation and/or the efficiency of their optimization algorithm. The most relevant architectures include Multi-Disciplinary Feasible (MDF) [5], Individual Discipline Feasible (IDF) [6], Collaborative Optimization (CO) [7] and Bi-Level Integrated Synthesis System (BLISS) [8].

The MDO research has matured in the last thirteen years, with the publication of many comparative studies. From [9] that compare several MDO methods, as for example the MDF and IDF, with five analytical examples of varying complexity or size, through [10] who used two application examples with the same metrics to evaluate three different MDO methods (CO, CSSO, and BLISS) or [11] who through the evaluation of different MDO architectures, using an extended set of metrics, demonstrated the promising features of evaluation metrics based both on the formulation considerations and on the optimization performance criteria.

In 1999, Reuther [12] published an article where an initial aero-structural analysis and optimization framework for MDO was presented. Later in 2002, Martins [13] developed that aero-structural analysis and optimization framework with a method to calculate the sensitivities of aerodynamic and structural cost functions with respect to both aerodynamic shape and structural variables that was both accurate and efficient. That framework coupled a linear finite-element structural model to a finite-volume Euler CFD solver and achieved a coupled

solution using a pseudo-time marching scheme with periodic updates of the displaced shape. A structural model composed of solid, three-dimensional elements was used to represent the stiffened aircraft wing. To transfer loads and displacements across the aircraft outer-mold line (OML), they used a systematic scheme based on the work developed by Brown [14]. Martins [15] developed a sensitivity analysis of the aero-structural equations for both the adjoint and direct formulations, with a block GaussSeidel technique for solving the coupled adjoint system.

Around the same time, Maute [16] presented an aero-structural analysis that coupled the Euler equations to a linear finite-element model, where, following the previous work of Maman [17], a mesh movement strategy based on a spring analogy and a load and displacement transfer technique was employed. Formulations of both the adjoint and direct methods for computing the sensitivities of the coupled aero-structural system were presented and, to solve the coupled nonlinear equations, they used a nonlinear block Gauss–Seidel method with relaxation. In 2004, Maute [18] developed an aero-structural optimization problem in which the internal structure of the wing box is parametrized using a single isotropic material with penalization approach to determine the topology of the optimal structure. The methods referred above were improved in terms of robustness and efficiency by Barcelos [19], who developed a class of Newton–Krylov–Schur methods for solving the coupled nonlinear fluid-structure-mesh movement problem. It consists of using an approximate Newtons method for the solution of the nonlinear coupled equations and of using a Schur complement approach at each iteration to solve the coupled linear system that results from a linearization of the residual. The same authors presented in 2008 [20] an aero-structural solution technique coupling the Navier–Stokes equations with a turbulence model to a linear structure and mesh movement strategy.

### 3 Implementation

#### 3.1 MDO Problem Definition

An MDO problem can be seen as a system containing multiple sub-systems, each dealing with a discipline governed by its own set of equations. A generalized representation of these equations is

$$y_i = f(x_i, y_j, z), \quad i, j = 1, \dots, n, \quad j \neq i, \quad (5)$$

where  $n$  is the number of disciplines,  $x_i$  is the local variable vector, the vector  $y_j$  corresponds to inter-disciplinary couplings, and  $z$  is the global variable vector.

When provided with a set of design variable inputs, the sub-systems will generate discipline feasible states and outputs. The set of inputs consist not only of disciplinary variables but also of coupling variables. The latter provide information regarding the state of the other disciplines.

The formulation of an MDO problem can be compared to a simple optimization problem as three entities need to be defined: the objective function, the design variables and the constraints.

An MDO problem has two main differences compared to a single disciplinary optimization problem that make it larger and more complex: 1) some disciplines need inputs that result from other disciplines; 2) some objective functions, design variables and constraints are shared by several disciplines.

In MDO problems, both the design variables and constraints can be classified, based on their effect in multiple disciplines, in local or global.

Ultimately, the way how an MDO problem is converted into one or more standard optimization problems is what defines the MDO strategy or architecture.

#### 3.2 MDO Architectures

A wide variety of MDO architectures have been proposed and evaluated, either by defining a different problem formulation or by finding the most efficient optimization algorithms [3]. The MDO architectures can be classified as:

- Single-level methods, like Individual Discipline Feasible (IDF) or Multi-Disciplinary Feasible design (MDF), include only one optimizer at a system-level, which runs a system analysis in each step and has authority over the global system [6];
- Multi-level methods, which include Concurrent Subspace Optimization (CSSO) [21] and Bi-level Integrated Systems Synthesis (BLISS) [8], create a subspace for each individual discipline, in which a local optimizer modified the design, and make use a global optimizer at the system-level, that manages the relationship between disciplines. These methods create a hierarchical structure in the global system, where each disciplinary sub-group was some degree of freedom to work independently.

The architecture is chosen taking into consideration several aspects, such as the number of the disciplines involved, the number and type of design variables, and the optimization method.

Comparison studies of the most common architectures [11, 22] showed MDF as the most accurate an robust method since it performs full disciplinary

system analysis and consistently return optimal solutions with the least number of failures. The efficiency of this architecture suffers with the increase in complexity, so it is better used with simple system analysis. Since the problem tackled in this work only deals with two disciplines, an MDF architecture was chosen.

### 3.3 Multi-Disciplinary Feasible

The MDF architecture is often viewed as the most traditional approach, where an optimizer is placed over an MDA module. The optimizer takes in the set of design variables, global  $z$  and local  $x$  variables, and iterates over the disciplinary analyses until a consistent set of coupling variables has been generated. Then, the complete variable set is used to compute the values of the objective and constraint functions.

The MDA is typically solved by a block-iterative procedure, like Gauss–Seidel, and is considered to be converged once the coupling variables remain constant within a specified tolerance over successive iterations. The fact that it requires a solution of the MDA at each design point, ensures that a multi-disciplinary feasible solution is present throughout the optimization process, so even if interrupted prematurely, a physically realizable design point will still be achieved. The computation of the MDA at each design point also negates the need to include the discipline coupling variables as optimization variables.

A schematic representation of the flow of information using MDF architecture is presented in Fig. 1.

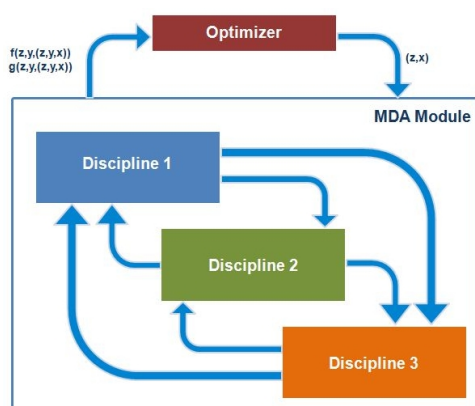


Figure 1: MDF architecture.

Mathematically, this architecture can be described as

$$\begin{aligned}
 &\text{Minimize} && f(z, y_i(x, y_j, z), x) \\
 &\text{w.r.t.} && z, x \\
 &\text{s.t.} && g(z, y_i(x, y_j, z)) \leq 0,
 \end{aligned} \tag{6}$$

where the indexes span  $i, j = 1, \dots, n, j \neq i$ , the objective function is denoted by  $f$ , and  $g$  represents the global and local system constraints.

## 4 MDO Framework

A modular structure was used in the present MDO framework. Figure 2 shows the scheme of the overall MDO tool structure established for the aerostuctural optimization of sailplane wings.

The numerical tools used were developed at the University of Toronto (UoT) MDO Lab [23]. The geometric parametrization method follows a CAD-free geometry parametrization approach [24]. The aerodynamic disciplinary solver consists of a panel code named *Tripán* and the structural solver is a parallel finite-element analysis package named *TACS*. The necessary coupling between these two solvers was already implemented.

As result of the choice of an MDF architecture only one global optimizer was needed. *SNOPT* [25], a sparse sequential quadratic programming (SQP) algorithm, was selected and it was fully integrated in the *pyOpt* MDO Lab module [26].

The interface between the modules was made in the Python scripting language since, even though the core components were mostly written in Fortran and C languages, they were wrapped in Python language.

### 4.1 Geometry Module

In aerodynamic analysis, a model of the wetted surface or outer mold line (OML) of the wing is required. On the other hand, the structural analysis of that same wing requires not only the OML but also a description of the internal structure components like ribs, skins, spars and stiffeners.

The CAD-free approach method uses both spline and free volume deformation (FFD) based approaches. The FFD volume base approach was first presented by Sederberg [27]. A good physical analogy that is often used to explain the FFD approach is the one where an object (or objects) that one wants to deform, is embedded in flexible material. The object itself is also assumed to be flexible, so that it deforms along (in a consistent motion) with the material surrounding it. The use of this technique allows easier parameterizations of solid object models since it is not the object geometry itself that is parametrized but rather the volume where it is embedded.

The tools used to implement the FFD approach include functionalities with both B-spline curves and surfaces and are called *pySpline* and *pyGeo*, respectively. *pySpline* is a underlying B-spline library for curves and surfaces. The wing geometry is then built by combining the resulting individual curves,

surfaces together in a topological manner using a geometry surfacing tool named *pyGeo*.

Given a description of the structural layout within the OML of the wing, another tool, named *pyLayout*, automatically generates a wing-box finite-element model that mimics the structural characteristics of the real wing.

## 4.2 Aerodynamics Module

Given that sailplanes fly in a low Mach number regime, the airflow can be modeled as incompressible. Also, as sailplanes are designed to be very streamlined, flow separation is hardly present and the viscous effects minimized. Therefore, it is a valid assumption to consider an inviscid, incompressible and irrotational model to accurately simulate flow.

The flow solver used, *Tripán*, is an unstructured, three-dimensional panel code that uses a first-order panel method with constant source and doublet singularity elements, distributed over the surface of a body, discretized with quadrilateral and triangular panels. This method allows the calculation of aerodynamic forces, moments and pressures for inviscid, incompressible, external lifting flows. Yet, it has well known limitations, especially of accuracy when computing drag.

To perform the aerodynamic analysis, *Tripán* determines the source strengths based on the onset flow conditions while the boundary conditions for the doublet strengths constitute a dense linear system, represented by

$$\mathbf{A}(u, w) = 0, \quad (7)$$

where  $u$  and  $w$  are the vectors of the structural and aerodynamic state variables.

The linear system represented in Eq. (7) is solved using the parallel, linear algebra routines in PETSc [28] and using the Krylov subspace method generalized minimal residual method (GMRES) [29]

with a block Jacobi Incomplete LU preconditioner formed using a sparse approximate-Jacobian.

## 4.3 Structures Module

The tool used for the structural analysis was a finite-element code developed by Kennedy [30] called Toolkit for the Analysis of Composite Structures (*TACS*). This code was created for the analysis of stiffened, thin-walled, composite structures using either linear or geometrically non-linear strain relationships. It can use higher-order finite-elements to enhance the stress prediction capability.

The residuals of the structural governing equations are expressed as

$$\mathbf{S}(u, w) = \mathbf{S}_c(u) - \mathbf{F}(u, w), \quad (8)$$

where  $u$  is a vector of displacements and rotations (structural state variables),  $w$  is a vector of aerodynamic state variables,  $S_c$  are the residuals due to conservative forces and internal strain energy and  $F$  are the forces due to aerodynamic loads.

The Jacobian of the structural residuals involves two terms. The first is the tangent stiffness matrix  $\mathbf{K} = \partial \mathbf{S}_c / \partial u$ . The second is the derivative of the force vector with respect to the structural displacements. These terms are computed using a matrix-free approach. Mathematically, the Jacobian of the structural residuals is represented by

$$\frac{\partial \mathbf{S}}{\partial u} = \mathbf{K} - \frac{\partial \mathbf{F}}{\partial u}. \quad (9)$$

*TACS* uses the Krylov subspace method GMRES and the Krylov method GCROT [31] to solve the non-symmetric, linear systems of Eq. (9).

It handles stress constraints by applying a local failure constraint at each Gauss point in the finite-element model. These local failure constraints compute a load factor,  $\lambda_k$ , required for that point to fail. The load factor implies that the current point will

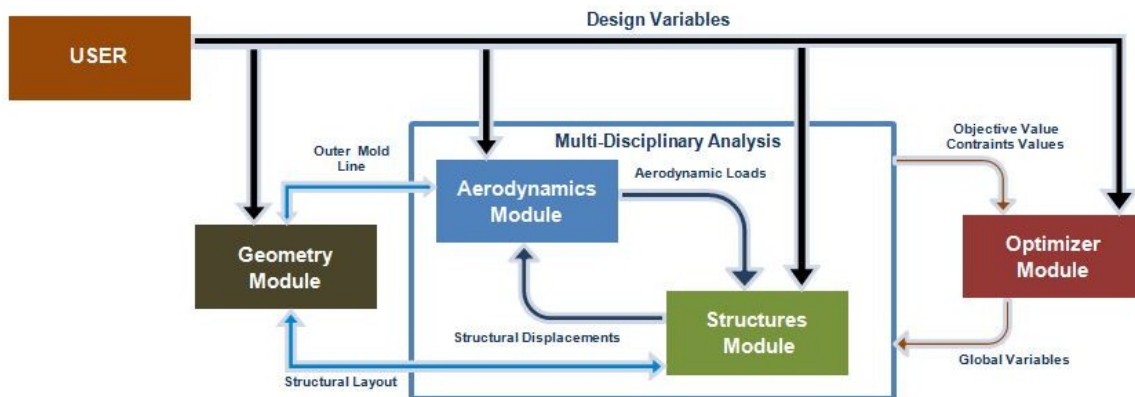


Figure 2: MDO tool structure established for the aero-structural optimization of sailplane wings.

fail at  $\lambda_k$  times the current stress level. For a safe-life design, the criterion  $\min \{\lambda_k\} > Fs$  is applied, where  $Fs$  is the safety factor. This method applied to an optimization has some specificities. Instead of using the minimum value directly, a Kreisselmeier-Steinhauser (KS) constraint aggregation technique is applied to groups of these local constraints [32]. Normally these groups are aggregated amongst similar structural components. In *TACS*, the KS function is computed as

$$\lambda_{KS} = \min \{\lambda_k\} - \frac{1}{\sigma} \ln \left[ \sum_{i=1}^N \exp \{-\sigma(\lambda_i - \min \{\lambda_k\})\} \right], \quad (10)$$

where  $\sigma$  is a weighting parameter that controls the degree of approximation and  $\lambda_{KS}$  is the aggregated KS value. This approach has the advantage that it reduces the number of constraints required in the optimization, while keeping a conservative approximation, in that  $\lambda_{KS}$  is a lower bound.

#### 4.4 Aero-Structural Coupling

The coupling between the two disciplines is made by a load and displacement transfer scheme that follows the method described by Brown [14].

The objective of the displacement process is to accurately translate the nodal displacements of the structural model to aerodynamic mesh point displacements. This method rely on extrapolation functions for the displacements of the internal structure to obtain the aerodynamic mesh displacements. These functions must satisfy two conditions:

- they must accurately reproduce a rigid body motion;
- the resulting aerodynamic mesh displacement field must be continuous over the whole surface.

To extrapolate the structural displacement field, each point of the aerodynamic mesh,  $\mathbf{x}_A$ , is associated to a point on the structural model,  $\mathbf{x}_S$ , so that the distance between the two points is minimized. The link between the points is made through the vector,  $\mathbf{r} = \mathbf{x}_A - \mathbf{x}_S$ , which maintains its position and orientation relative to the associated finite-element point. The displacement of the aerodynamic mesh point,  $\mathbf{u}_A$ , can then be expressed as

$$\mathbf{u}_A = \mathbf{u}_S - \mathbf{r} \times \boldsymbol{\theta}_S, \quad (11)$$

where  $\mathbf{u}_S$  is the displacement of the structural model point, and  $\boldsymbol{\theta}_A$  and  $\boldsymbol{\theta}_S$  are equal rotations.

The load transfer procedure is similar to the displacement transfer. The pressures calculated by the aerodynamic flow solver are transferred to the structural nodes through aerodynamic mesh points. To perform the transfer, an appropriate cell and

the parametric location of each mesh point within this cell are identified. The aerodynamic pressures are then calculated by bilinear interpolation on the surface of the aerodynamic mesh. The distributed pressure load, applied to a structural finite-element model, must first be transformed into an equivalent set of nodal forces. This transformation has two requirements:

- the resultant nodal forces and moments are the same as those that result from the pressure field for each element;
- the load transfer must be conservative.

To ensure the former, the virtual work performed by the load vector,  $\mathbf{f}$ , undergoing a virtual displacement of the structural model,  $\delta u$ , must be equal to the work performed by the distributed pressure field,  $p$ , undergoing the equivalent displacement of the aerodynamic mesh,  $u_A$ ,

$$\delta W_S = \delta W_A. \quad (12)$$

#### 4.5 Aero-Structural Solution

The coupled non-linear system of equations is a combination of the aerodynamic and structural residuals, Eqs.(7) and (8), respectively, represented by

$$\mathbf{R}(q, x) = \begin{bmatrix} \mathbf{A}(w, u, x) \\ \mathbf{S}(w, u, x) \end{bmatrix} = 0, \quad (13)$$

where,  $x$  is the set of design variables and  $q$  is the combination of aerodynamic and structural states,  $q^T = [w^T u^T]$ . During the solution procedure, a point is considered converged when the relative tolerance of both residuals is reduced below a specified tolerance.

To solve the aero-structural system in Eq. (13), an approximate Newton-Krylov method is used. This method results in the linear system of equations for the update,  $\Delta q^{(n)}$ , expressed as

$$\frac{\partial \mathbf{R}}{\partial q} \Delta q^{(n)} = -\mathbf{R}(q^{(n)}). \quad (14)$$

This method can converge quadratically if the starting point is sufficiently close to the solution and the Jacobian remains non-singular. However, to achieve convergence when the starting point is far from the solution, the method may have to be globalized with some strategy, to ensure progress is made towards the solution until a suitable starting point is found. So, solving Eq. (14) inexactly for each update is typically more efficient than finding an accurate solution.

## 4.6 Optimizer

In design optimizations, like those in aircraft, that feature a large number of design variables, expensive high-fidelity analyses and a smooth design space, the benefit goes for the gradient-based methods. These methods have the advantage that it requires a smaller number of function evaluations to converge to the optimum.

The optimization algorithm used is called *SNOPT* [25]. This module has been compiled with a Python interface, named *pySNOPT*, for an easy integration in the MDO framework.

Efficient gradient-based optimization requires the accurate and efficient computation of the objective and constraint gradients. Following [13], an aerostuctural adjoint method that is based entirely on analytical derivatives was used. The implicit aerostuctural adjoint equations are

$$\frac{\partial \mathbf{R}^T}{\partial q} \psi = \frac{\partial f}{\partial q}, \quad (15)$$

where  $\psi$  refers to the adjoint vector and  $f$  is either an aerodynamic or structural function of interest. Once the adjoint vector  $\psi$  has been determined using Eq. (15), the total derivatives are computed using

$$\frac{df}{dx} = \frac{\partial f}{\partial x} - \psi^T \frac{\partial \mathbf{R}}{\partial x}. \quad (16)$$

## 5 Results

### 5.1 Case Study

The case study chosen is the LET L-23 Super Blaník sailplane wing. This is an all-metal, cantilever, mono-spar, tapered wing that consists of two assemblies. Its main geometry parameters are summarized in Tab. 1.

Table 1: Geometry parameters for the case study.

Parameter	LET L-23	
Span	16.2	<i>m</i>
Reference Area	19.15	<i>m</i> <sup>2</sup>
Taper Ratio	0.429	
Dihedral Angle	3	°
Sweep Angle	-5	°
Twist Angle	-3	°

The real structural layout of the L-23 wing [33] was used as reference for its structural modeling. Therefore, the wing internal layout is modeled with seventeen ribs, one main spar and an auxiliary spar. The thickness values for the structural components were set to 5mm in the skin, 10mm in the spars and 8mm in the ribs. Although it is not the exact

modeling of the real layout, it was the best approximation that was possible to recreate using the geometry module. Also, a maximum take-off weight of 530kg was considered.

Figure 3 shows the geometry objects created for the L-23 case study. As observable, the aerodynamic meshes are almost perfectly coincident with the OML of the desired wing geometry. Also, the structural models of the wing box fits perfectly in the OML.

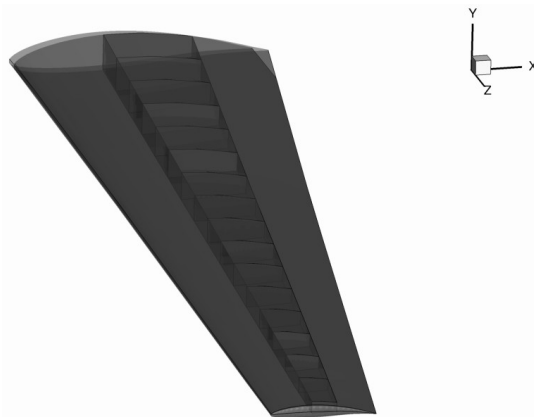


Figure 3: Geometry objects for the L-23 case study.

### 5.2 Aerodynamics

The free-stream conditions were chosen to match those of a cross-country soaring flight at 1000m, with a velocity of 25m/s. Table 2 summarizes the free-stream conditions defined in the simulation.

Table 2: Flow conditions for aerodynamic analysis.

Parameter		
Mach	0.074	
Angle of Attack	3	°
Density	1.112	<i>Kg/m</i> <sup>3</sup>
Speed of Sound	336.4	<i>m/s</i>

#### 5.2.1 Verification and validation of *Tripan*

To verify the fidelity of the aerodynamics simulation code *Tripan*, another CFD code was used. *SUmb*, a multi-block structured flow solver developed in the Center for Integrated Turbulence Simulations (CITS) at Stanford University, was chosen for this task. It is a code that solves the compressible Euler, laminar Navier–Stokes and Reynolds-Averaged Navier–Stokes equations [34] and has been extensively validated using experimental data.

The wing geometry used to perform the comparison analysis was the ONERA M6 wing, a swept,

semi-span wing with no twist, that has a symmetric airfoil. The semi-section of the airfoil is the ON-ERA D section [35].

To this purpose an incompressible, inviscid external flow was used. A sample of the results for the *Tripan* validation is shown in Fig. 4 presenting the  $C_p$  distribution at the 85% wing span section.

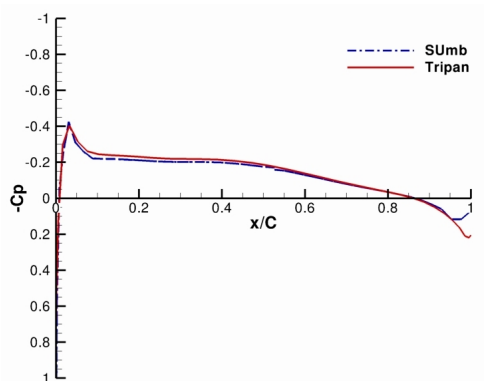


Figure 4: *Tripan* verification results at 85% span.

Results show that the two numerical flow solvers produce results very close to one another. Only in the trailing-edge, a slightly difference is noted. The agreement between solvers attest that *Tripan* provides accurate results when simulating incompressible inviscid flows.

### 5.2.2 Mesh Convergence Study

Before running the aerodynamic analysis, a convergence study was performed to determine the proper number of panels for the aerodynamic mesh discretization. A range of *Tripan* objects was created from a coarse mesh with 150 panels, to a highly refined mesh with 12,150 panels. Then, an aerodynamic analysis was performed on each mesh. To assess the results obtained, a relative error evaluation was performed using the value computed for the most refined mesh as reference, given that the real value of the aerodynamic quantities was not known. A graphic with the convergence of the results was compiled and presented in Fig. 5.

As *Tripan* uses a panel code, the error for the lift coefficient converges much faster than the drag coefficient. Although the computed drag value is not accurate, as the code can not compute the total drag, it was important to assess its convergence. Also, the time required to perform the aerodynamic analysis was measured. It is observable that time grows linearly with the number of panels used.

From the results seen, a panel number near 7,000, was considered to give the best relation between accuracy error (approximately 10%) and time to perform the analysis (approximately two minutes).

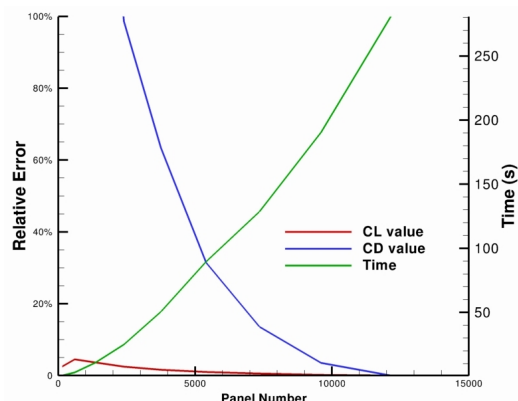
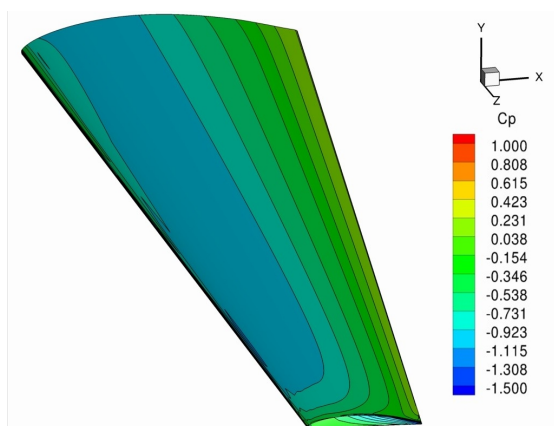


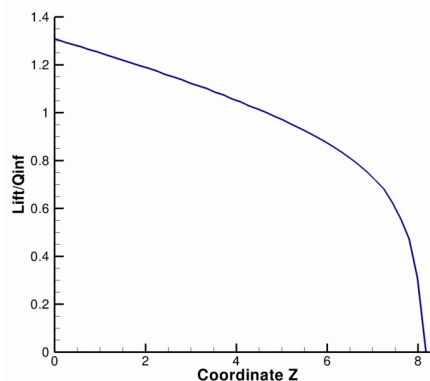
Figure 5: Convergence study on *Tripan* mesh.

### 5.2.3 Aerodynamic Analysis

With every parameter defined, the aerodynamics module was used to perform the aerodynamic analysis of the case study. Figure 6 summarizes the results obtained, which consist of  $C_p$  distribution over the wing and lift distribution across the wing span.



(a)  $C_p$  distribution.



(b) Lift distribution.

Figure 6: Aerodynamic analysis results.

These results show that the lift distribution dif-

fers from the theoretical aerodynamic elliptical optimum. Yet, if one accounts for the fact that, although tapered, the L-23 wing also has a constant twist and sweep angles, then the results seem more comprehensive. The L-23 having more inboard lift results in a smaller bending moment at the wing root, thus enabling the use of lighter structural components. This is a clear evidence that structures were taken into account when the wing was designed by the manufacturer.

As for the  $C_p$  distribution, it shows smooth gradients as expected since the L-23 wing airfoil morphs from a NACA 63<sub>2A</sub>-615 at root to NACA 63<sub>2A</sub>-612 at tip (both laminar airfoils). It is clear that the airfoils in the L-23 wing have been chosen to provide good results in low speed gliding performance.

#### 5.2.4 Aerodynamic Optimization

One of the main objectives in sailplane performance is the maximization of the  $L/D$  ratio, to maximize the flight range. The initial flight condition for the optimization is the same as that of the aerodynamic analysis, presented in Tab. 2. The objective function was the  $L/D$  ratio and a lift constraint was imposed through  $C_L$  to enforce level-flight ( $L = W$ ).

With the lift constrained, the range optimization problem translates into a drag minimization problem. A total of nine variables were chosen as design variables: angle-of-attack, four twist angles and four chord scale factors. The span is fixed to the initial value. A summary of the initial and final parameters of the aerodynamic optimization is shown in Tab. 3.

The results verify that, although the initial  $C_L$  was different from the required value, the constraint was fulfilled in the optimization process. The initial  $C_L$  value was higher than required so the angle-of-attack did not have to be increased which allowed the optimizer to start from the beginning making changes to lower the drag, as illustrated in Fig. 7.

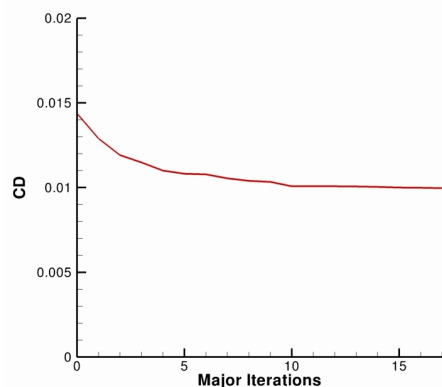
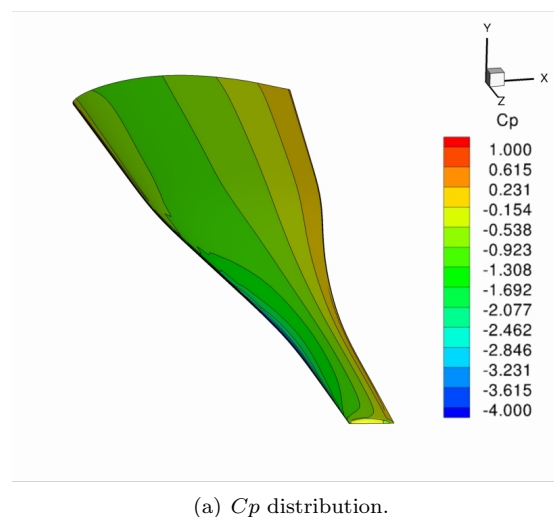


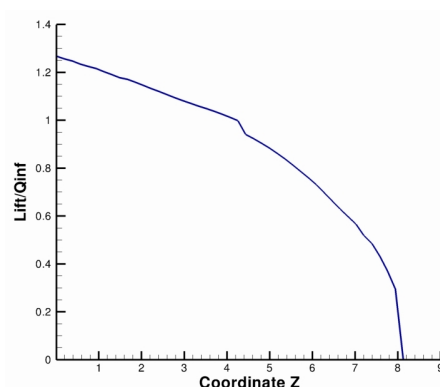
Figure 7: Convergence history for the aerodynamic optimization.

The values of twist and chord changed as well. The twist group of variables shows that once reached a sufficient angle-of-attack, the optimizer chose to increase the twist angle of the middle sections. Although the final twist values had to be adjusted, since the real wing has a  $-3^\circ$  twist, it is clear that the optimizer changed the twist angles so that a lift distribution closer to the aerodynamic optimal could be reached, therefore, reducing the drag. As for the chord group of variables, it shows a decrease as the sections approach the wing tip. That corresponds to inserting even more taper to the already initially tapered geometry. From an aerodynamic perspective, that was expected since taper ratio leads to a lift distribution closer to elliptical. Also, because the span was fixed, reducing the wing chord, reduced the overall wing area, which increased the aspect ratio of the wing.

Fig. 8 shows the lift and  $C_p$  distribution over the wing surface of the aerodynamically optimized L-23 wing.



(a)  $C_p$  distribution.



(b) Lift distribution.

Figure 8: Aerodynamic optimization results.

The difference between the initial and the optimized aerodynamic parameters proves once again that the real L-23 wing resulted from a design pro-

Table 3: Aerodynamic optimization parameters for the L-23 wing.

Parameter	Initial Value	Optimized Value	Lower Bound	Upper Bound	
$C_L$	0.981	0.779	0.779	0.779	
Angle-of-Attack	3	3.15	-4	7	°
Twist (z/b=30%)	0	0	-10	10	°
Twist (z/b=60%)	0	5	-10	10	°
Twist (z/b=90%)	0	5	-10	10	°
Twist Tip	0	-5	-10	10	°
Chord Scale (z/b=30%)	1	1	0.5	2	
Chord Scale (z/b=60%)	1	0.5	0.5	2	
Chord Scale (z/b=90%)	1	0.5	0.5	2	
Chord Tip	1	0.5	0.5	2	
$C_D$	0.0143	0.0100			

cess that took other disciplinary constraints into account.

### 5.3 Structures

The structural simulation performed consisted of the analysis of the stresses and deformations of the wing-box when subjected to a single vertical wing tip nodal load of  $500N$ . The mechanical properties used for all the wing structures were based on Aluminum 7075, a reference in the aeronautic industry, whose mechanical properties are listed in Tab. 4.

Table 4: Mechanical properties of Aluminum 7075.

Properties		
Density	2810	$Kg/m^3$
Young's Modulus	71.7	$GPa$
Poisson's Ratio	0.33	
Correlation Factor	0.8333	
Yield Strength	434	$MPa$

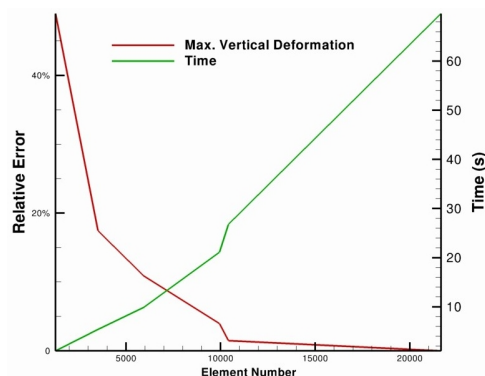
The finite-elements used for the structural mesh are based on mixed interpolation of tensorial components approach (MITC) shell elements [36] and the internal structural layouts.

#### 5.3.1 Mesh Convergence Study

To determine how many elements are needed to have a reliable structural mesh discretization, a convergence study was performed using an academic semi-tapered wing as chosen layout.

A set of finite-element structural meshes, ranging from 6,000 to 22,000 elements was tested and the tip vertical displacement used as monitored output. Figure 9 shows the results of this convergence study. Similarly to Sec. 5.2.2, the relative error was used to assess the accuracy, and the value obtained using the finest mesh used as reference.

The results presented in Fig. 9 show that the run time grows almost linearly with the number of elements used. A total number of elements above


 Figure 9: Convergence study on *TACS* mesh.

7,500 was considered to give the best relation between accuracy error (approximately 10%) and time to perform the analysis (approximately 13 seconds).

#### 5.3.2 Structural Analysis

Using the methodology previously described, the structural analysis of the case study was performed.

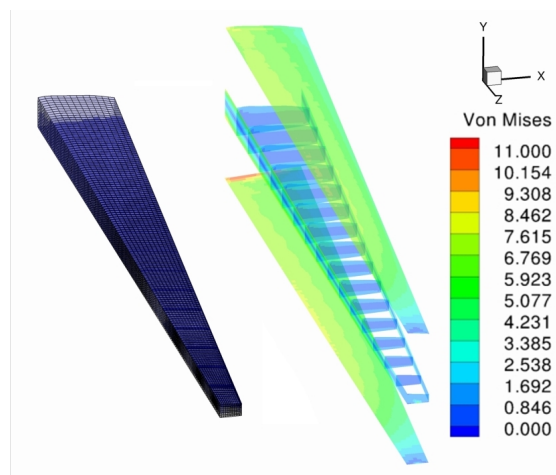


Figure 10: Structural analysis results.

Despite the span of the L-23 wing-box being greater than most sailplane aircrafts, it showed very little deformation as illustrated in Fig.10. That result was already expected since the structure layout is based on the real L-23 wing-box, which has high stiffness due to its high number of ribs, contributing to the overall structure resistance to bending. Again, the wing shows aspects that justify why the L-23 sailplane is so highly regarded for its robustness.

The other results studied were the Von Mises stresses. These give information about how much effort are the different structural components sustaining. As Fig. 10 shows, the values of the Von Mises stresses are very small. The maximum values are verified in the lower skin panels at the wing-box root, probably caused by the sweep, twist and dihedral angles applied to the wing-box. The higher height of the wing-box also allows the observation of zones that are sustaining higher stresses within the ribs.

These results highlighted the good starting structural design point that the L-23 wing case is. Although simple, these observations are important in the preliminary design stage, as they can allow the early choice of the better overall structure layout for the main components of the sailplane wing.

#### 5.4 Aero-Structural Optimization

After having successfully tested the different MDO framework modules, the aero-structural optimization could be performed. The initial flight conditions used were the same as those used for the aerodynamic and structural analysis of Secs 5.2.3 and 5.3.2.

In addition to the maximization of the  $L/D$  ratio, the weight minimization is one of the main objectives in sailplane performance since it maximizes flight endurance. As such, the MDO optimization problem consisted of drag minimization with a weight constraint which enforced the total weight reduction.

Two types of constraints were set: 1) an aerodynamic constraint forcing the lift generated by the wing to match the sailplane weight; 2) a structural constraint for the maximum Von Mises stresses. The sailplane weight was not fixed, since reducing the weight of the wing structure was one of the objectives. Instead, a percentage of the initial weight of the sailplane was fixed, allowing the remaining percentage to change according to the wing structural weight. The Von Mises stress constraints were imposed indirectly through four KS functions, which aggregated all stresses into a four individual constraints, corresponding to the top skin, bottom skin, spar and rib group elements. These were set to the range of 0.3 to 2.

The design variables included structural component thicknesses, allowing the reduction of the weight, and aerodynamic parameters (angle-of-attack, twist and chord at four different sections), allowing variation of lift.

The results of the aero-structural optimization are summarized in Tab. 5, where a comparison of the initial and optimized design variables and constraints is presented. As the number of thickness variables was too long, a median was made for each group of components.

The results of the aero-structural optimization show that its objective was achieved, which was the drag minimization subjected to aerodynamic and structural constraints, enforcing the weight reduction of the structure. Looking to the optimization constraints, all of them have been fulfilled, so a feasible design was generated in the optimization.

The aerodynamic parameters show some important aspects of the optimization. The most notorious is the optimized angle-of-attack, that is lower than the initial, to decrease the lift generated. The resulting drag decrease is visible in Fig. 11.

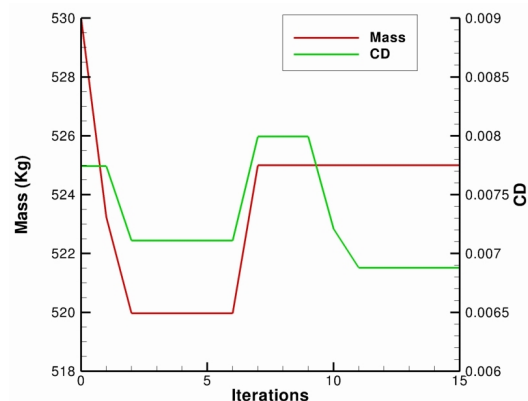


Figure 11: Convergence history for the aero-structural optimization.

The chord of the sections along the span was decreased, leading to a wing with higher taper ratio. In contrast to the aerodynamic optimization in Sec. 5.2.4, the chord values were not lowered to the minimum allowed because, as the objective was also weight reduction, some trade-offs had to be made between the aerodynamic and structural performance. This fact also explains the fluctuations in the drag values during the convergence history. In addition, decreasing the chord of the wing sections to lower values would have implications in the structural stiffness of the wing box and, therefore, in the values of the KS constraints.

The structural parameters are consistent with the constraint values. The median thickness of the top skin, bottom skin and spar groups were lowered to values close to the minimum possible, there-

Table 5: Aero-structural optimization parameters for the L-23 wing.

Parameter	Initial Value	Optimized Value	Lower Bound	Upper Bound	
Total Mass	530	525	0	525	<i>Kg</i>
KS top skin group	-	0.340	0.3	2	
KS bottom skin group	-	0.358	0.3	2	
KS spar group	-	0.353	0.3	2	
KS rib group	-	2	0.3	2	
Angle-of-Attack	3	1.24	-4	7	°
Twist (Four Sections)	0	5	-10	10	°
Chord Scale (Four Sections)	1	0.768	0.5	2	
Median Top Skin Thickness	5	1.5	1.5	10	<i>mm</i>
Median Bottom Skin Thickness	5	1.5	1.5	10	<i>mm</i>
Median Spar Thickness	5	5	5	10	<i>mm</i>
Median Rib Thickness	8	10	1.5	10	<i>mm</i>
$C_D$	0.00774	0.00687			

fore reducing the stresses sustained by these components and the value of their KS functions (lowering the associated safety factor). However, the median rib thickness was increased, probably to satisfy the structural constraints. By increasing the rib thickness, the stresses sustained decreased such that their KS functions would be within the constraint bounds. This explains why the KS function value of the rib group is at the higher bound and why the weight has been optimized to the higher bound value.

These findings highlight the trade-off made by the optimizer between lowering the structural weight and fulfilling the structural constraints. Figures 12 and 13 show the results of the aero-structural optimization.

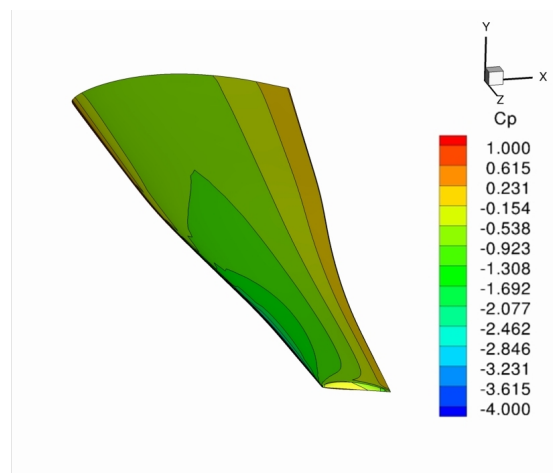
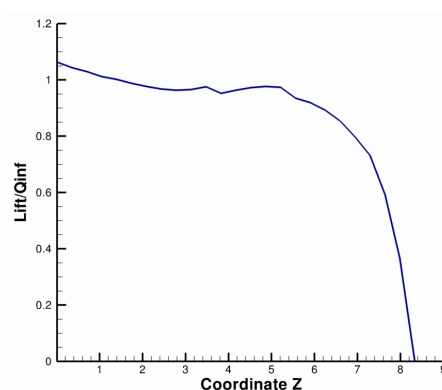
Differences from the simple disciplinary optimizations were evident, proving once again that some trade-offs had to be made between the structural performance and the aerodynamic performance.

Looking at Fig. 13, one can see the higher deformation of the wing-box when compared to the simple structural analysis exercise. Also the higher Von Mises stresses show that a higher effort is being made by the structural components. These results are consistent with the minimum KS function values, which corresponds to the top and bottom skin groups. The changes in lift and  $C_p$  distribution over the wing were caused by a lower angle-of-attack in the root sections and a higher angle-of-attack in the tip sections (due to the local twist applied).

Ultimately, the optimization problem was successfully accomplished, as the objective of reducing the weight and drag of the sailplane were achieved while fulfilling the structural and aerodynamic constraints.

## 6 Conclusions

A multi-disciplinary design of aircraft wing considering the two core disciplines — aerodynamics and


 (a)  $C_p$  distribution.


(b) Lift distribution.

Figure 12: Aero-structural optimization results.

structures — was performed. The MDO framework was laid down using an MDF architecture and its module capabilities described to same detail. These different modules were initially tested individually before being exercised in the coupled framework.

Even though the exercises performed were relatively simple, the approach to aero-structural design optimization was generic and can easily be ex-

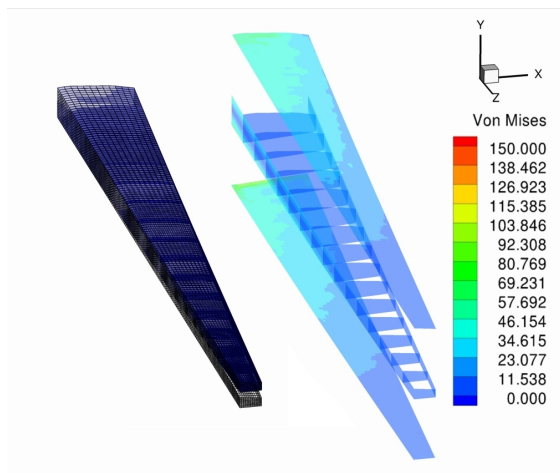


Figure 13: Deformation and Von Mises stresses of the wing structural layout.

tended to other test cases. It should be mentioned that formulation of the aero-structural problems was the hardest task, which demonstrates the difficulties found by the aircraft industry in adopting formal MDO approaches into their design processes.

From the results obtained with the aero-structural optimization, it was possible to capture the multi-disciplinary trade-offs between what was best in terms of aerodynamics and what was feasible in terms of aero-structural requirements. Having this multi-disciplinary perspective right from the beginning of the design process can reduce the feasible design space, allowing resources to be saved from later re-designs. This highlighted the importance of using MDO in a preliminary stage of an aircraft design.

Future work is expected in two fronts: 1) in the formulation of the multi-disciplinary problem, to consider other objective or constraint functions that inherently couple the disciplines, and to handle multiple flight conditions simultaneously; 2) in the different modules of the MDO framework, so that even more realistic aircraft design problems can be solved, dealing with transonic flow and composite materials.

Another task to be considered will be the a validation of some results with some experimental tests, for example with the Portuguese Air Force sailplanes.

### Acknowledgements

The authors would like to thank Dr. Graeme Kennedy for the support and availability to help with the MDO toolset usage.

### References

- [1] Portuguese Air Force. PERSEUS - Protection of European borders and Seas through the intelligent Use of Surveillance. <http://www.academiafa.edu.pt/index.php?bd0b6f49=011.005.002>, 2010. Accessed October 2011.
- [2] Portuguese Air Force. PITVANT - Project for Research and Technology in Unmanned Aerial Vehicles. <http://www.academiafa.edu.pt/index.php?bd0b6f49=011.005.004>, 2009. Accessed October 2011.
- [3] MDO Technical Committee, editor. *Current State of the Art in Multidisciplinary Design Optimization*. AIAA White Paper, Reston VA, January 1991.
- [4] J. Sobieszczanski-Sobieski. Multidisciplinary design optimization: An emerging new engineering discipline. In *Proceeding of the World Congress of Optimal of Structural Systems*, August 1993.
- [5] Cramer. Problem formulation for multidisciplinary optimization. In *SIAM Journal of Optimization*, 4, pages 754–776, November 1994.
- [6] J.E. Dennis and R.M. Lewis. Problem formulations and other optimization issues in multidisciplinary optimization. In *AIAA Symposium on Fluid Dynamics*, Colorado Springs, CO, June 1994. AIAA paper 94-2196.
- [7] R. Braun, P. Gage, I. Kroo, and J. Sobieszczanski-Sobieski. Implementation and performance issues in collaborative optimization. In *Proceedings 5th AIAA/USAF MDO symposium*, Bellevue, WA, September 1996. AIAA Paper 96-4017.
- [8] J. Sobieszczanski-Sobieski, S. A. Jeremy, and R. S. Jr. Robert. Bi-level integrated system synthesis (BLISS). In *National Aeronautics and Space Administration Technical Manual*, NASA/TM-1998-208715. AIAA, August 1998.
- [9] K.F. Hulme and C.L. Bloebaum. A comparison of solution strategies for simulation-based multidisciplinary design optimization. In *Proceedings Seventh AIAA/NASA/ISSMO Symposium on Multidisciplinary Analysis and Optimization*, St. Louis, MO, September 1998. AIAA Paper 98-4977.
- [10] S. Chen, F. Zhang, and M. Khalid. Evaluation of three decomposition MDO algorithms. In *Proceedings of 23rd International Congress of Aerospace Sciences*, Toronto, Canada, September 2002. AIAA.
- [11] R. Perez, H. H. T. Liu, and K. Behdinin. Evaluation of multidisciplinary optimization approaches for aircraft conceptual design. In *AIAA/ISSMO Multidisciplinary Analysis and Optimization Conference*, Albany, NY, September 2004.

- [12] J. J. Reuther, J. J. Alonso, J. R. R. A. Martins, and S. C. Smith. A coupled aero-structural optimization method for complete aircraft configurations. *AIAA paper 99-0187*, 1999.
- [13] J. R. R. A. Martins. *A coupled-adjoint method for high-fidelity aero-structural optimization*. Ph.d. thesis, Stanford University, Stanford, CA, October 2002.
- [14] S. Brown. Displacement extrapolation for CFD+CSM aeroelastic analysis. *AIAA Paper 97-1090*, 1997.
- [15] J. R. R. A. Martins, J. J. Alonso, and J. J. Reuther. A coupledadjoint sensitivity analysis method for highfidelity aerostructural design. In *Optimization and Engineering*, volume 6, pages 33–62, 2005.
- [16] K. Maute, M. Nikbay, and C.Farhat. Coupled analytical sensitivity analysis and optimization of three-dimensional nonlinear aeroelastic systems. In *AIAA Journal*, volume 39, pages 2051–2061, 2001.
- [17] N. Maman and C. Farhat. Matching fluid and structure meshes for aeroelastic computations: a parallel approach. In *Computers and Structures*, volume 54, pages 779–785, 1995.
- [18] K. Maute and M. Allen. Conceptual design of aeroelastic structures by topology optimization. In *Structural and multi-disciplinary optimization*, volume 27, pages 27–42, 2004.
- [19] M. Barcelos, H. Bavestrello, and K. Maute. A Schur-Newton-Krylov solver for steady-state aeroelastic analysis and design sensitivity analysis. In *Computer Methods in Applied Mechanics and Engineering*, volume 195, pages 2050–2069, 2006.
- [20] M. Barcelos and K. Maute. Aeroelastic design optimization for laminar and turbulent flows. In *Computer Methods in Applied Mechanics and Engineering*, volume 197, pages 1813–1832, 2008.
- [21] J. Sobieszczanski-Sobieski. Optimization by decomposition: A step from hierarchic to non-hierarchic systems. Technical report, NASA Technical Report CP-3031, 1988.
- [22] N. P. Tedford and J. R. R. A. Martins. Benchmarking multidisciplinary design optimization algorithms. *Optimization and Engineering*, 11(1):159–183, 2009.
- [23] MDO Laboratory of UoT. Official website for the multidisciplinary optimization laboratory of University of Toronto. <http://mdolab.utias.utoronto.ca/>, 2000. Accessed September 2011.
- [24] Gaetan K.W. Kenway, Graeme J. Kennedy, and Joaquim R. R. A. Martins. CAD-free approach to high-fidelity aerostructural optimization. *13th AIAA/ISSMO Multidisciplinary Analysis Optimization Conference*, pages 1–3, Sep 2010.
- [25] Philip E. Gill. *Users Guide for SNOPT Version 7: Software for Large-Scale Nonlinear Programming*. Department of Mathematics of University of California, San Diego, CA, June 2008.
- [26] Ruben E. Perez, Peter W. Jansen, and Joaquim R.R.A. Martins. pyOpt: A Python-based object-oriented framework for nonlinear constrained optimization. *Structures and Multi-disciplinary Optimization*, 2011.
- [27] T. W. Sederberg and S. R. Parry. Free-form deformation of solid geometric models. *SIGGRAPH Comput. Graph.*, 20:151160, 1986.
- [28] Satish Balay, Kris Buschelman, Victor Eijkhout, William D. Gropp, Dinesh Kaushik, Matthew G. Knepley, Lois Curfman McInnes, Barry F. Smith, and Hong Zhang. PETSc users manual. Technical Report ANL-95/11 - Revision 2.3.0, Argonne National Laboratory, 2004.
- [29] Y. Saad and M. H.Schultz. GMRES: A generalized minimal residual algorithm for solving nonsymmetric linear systems. *SIAM Journal on Scientific and Statistical Computing*, 7(3):856869, 1986.
- [30] Graeme J. Kennedy and Joaquim R. R. A. Martins. Parallel solution methods for aerostructural analysis and design optimization. *13th AIAA/ISSMO Multidisciplinary Analysis Optimization Conference*, Sep 2010.
- [31] J.E. Hicken and D.W. Zingg. A simplified and flexible variant of GCROT for solving nonsymmetric linear systems. *SIAM Journal on Scientific Computing*, 32(3):1672–1694, 2010.
- [32] G. Wrenn. An indirect method for numerical optimization using the Kreisselmeier-Steinhauser function. Nasa technical report cr-4220, National Aeronautics and Space Administration, 1989.
- [33] LET Aircraft Industries. *L-23 Super-Blanik Sailplane Maintenance Manual*. Portuguese Air Force, 2011.
- [34] Edwin Van Der Weide, Georgi Kalitzinand, J.Schliter, and Juan J. Alonso. Unsteady turbomachinery computations using massively parallel platforms. In *44th AIAA Aerospace Sciences Meeting and Exhibit*, Reno, NV, January 2006. AIAA Paper 2006-421.
- [35] V. Schmitt and F. Charpin. Pressure distributions on the ONERA-M6-wing at transonic mach numbers. *Experimental Data Base for Computer Program Assessment. Report of the Fluid Dynamics Panel Working Group 04, AGARD AR 138*, May 1979.
- [36] D. Chapelle, D.L. Oliveira, and M.L. Bucalem. MITC elements for a classical shell model. *Comput. & Structures*, 81:523–533, 2003.